A Tendon-Driven Origami Hopper Triggered by Proprioceptive Contact Detection

Wei-Hsi Chen*, Shivangi Misra‡, J. Diego Caporale†,
Daniel E. Koditschek*, Shu Yang⋆, Cynthia R. Sung†

***Abstract*— We report on experiments with a laptop-sized (0.23m, 2.53kg), paper origami robot that exhibits highly dynamic and stable two degree-of-freedom (circular boom) hopping at speeds in excess of 1.5 bl/s (body-lengths per second) at a specific resistance $O(1)$ while achieving aerial phase apex states 25% above the stance height over thousands of cycles. Three conventional brushless DC motors load energy into the folded paper springs through pulley-borne cables whose sudden loss of tension upon touchdown triggers the release of spring potential that accelerates the body back through liftoff to flight with a 20W powerstroke, whereupon the toe angle is adjusted to regulate fore-aft speed. We also demonstrate in the vertical hopping mode the transparency of this actuation scheme by using proprioceptive contact detection with only motor encoder sensing. The combination of actuation and sensing shows potential to lower system complexity for tendon-driven robots.**

I. Introduction

This paper presents a tendon-driven, parallel-spring hopping machine [1] whose leg kinematics and compliance are simultaneously provided by an origami structure [2] to reduce design complexity while overcoming the challenges in energy loss associated with current soft locomotion machines. Opening legged robots to the emerging design space of algorithmic metatmaterials [3] promises still greater future benefit from active, pluripotent components.

A. Motivation

Dynamic robots — machines capable of managing the kinetic as well as the potential energy of their bodies and environments — can manipulate objects using fewer actuated degree-of-freedom (DoF) [4] than and negotiate environments otherwise inaccessible [5] to quasi-statically operated mechanisms. Compliance has long been understood to play a key role in both quasi-static [6] and dynamic manipulation [7] and locomotion [8], [9], [10], where it improves both the passive stability [11], [12] and energetic efficiency [13], [14], [15] of the robot compared to rigid designs. However, due to the high speeds and impacts involved, implementing compliance in a robot using traditional means is often costly both in material weight and volume.

The integration of "soft" materials [16], [17] offers the promise of simpler, more robust yet tunable compliance mechanisms than those achieved by conventional rigid components [18]. However soft materials are also typically lossy, hence soft robots are generally slow and operated in the quasi-static regime [19], [20]. The fastest soft ground locomotion robot[1] we are aware of, [23][2], transports its $10^{-1}\,\mathrm{kg}$ body at a maximum speed of $0.5\,\mathrm{bls}^{-1}$ (body-lengths per second). Even if speed is not intrinsically valued in every application, efficiency at load is always important: the absence of power data in the soft robot locomotion literature precludes our making quantitative comparisons, but we presume that cost of transport [24], [25] of such small loads at such slow speeds will be orders of magnitude larger than the $O(1)$ range of specific resistance (SR) regularly achieved and increasingly improved [26], [27] by conventional legged machines.

B. Related Work

1) Origami Robots: Origami structures, meta-materials formed by folding flat sheets, exhibit compliance and resilience properties distinct from those of the planar constituent material as a result of the folding pattern and geometric constraints [28], [29]. Origami designs reported in the literature, prior to our recent origami juggler [30], store energy only in the folds and can achieve dynamic manipulation either with very small loads [31], [32] or through the use of additional springs [33]. Our juggler [30] and its (essentially merely inverted) operation as the hopper reported here (along with a highly resilient single shot leaping machine [34]) perform considerably larger work due to the new Reconfigurable Expanding Bistable Origami (REBO) pattern [2] that recruits bending energy from the faces, which would have previously been considered rigid plates. We show in Sec. IV-B that the resulting REBO hopper achieves a specific resistance of 1.6[3].

2) Proprioception: At the same time, we demonstrate that the intrinsic compliance of the hopper enables contact detection through proprioception, allowing us to translate sensor-minimal approaches to contact detection from conventional robot designs to our highly dynamic tendon-driven

*Department of Electrical and Systems Engineering, ‡Department of Computer and Information Science, †Department of Mechanical Engineering and Applied Mechanics, ⋆Department of Materials Science and Engineering, University of Pennsylvania, General Robotics, Autonomous, Sensing and Perception (GRASP) Lab

[1]One-shot explosive soft robots as in [21], [22] are not considered.

[2]Rough estimates from the clues we found in this paper suggest it operates at least two orders of magnitude greater potential ($\sim 10^{-2}$J) than kinetic ($\sim 10^{-4}$J) energy, confirming its quasi static nature. We hope the present paper encourages future soft robotics authors to include more careful energetic analysis to better facilitate comparison between and advances beyond present day locomotion technologies.

[3]Note this figure is computed with reference to the mechanical power output over a hop rather than the electrical supply power required over a certain distance, similar to the arguments made in [25].

robot. Making and breaking contact with the surfaces in an environment is a ubiquitous feature of dexterous robotics, but the challenge of engineering timely and accurate estimates of such events has prompted decades of effort to avoid [35] or minimize [36] the need to sense them. It is possible for robots to run in steady state with minimal sensing [37], and mechanically well designed legs can provide reliable ground contact even on complex substrates [38], [39]. However, effective control of both steady-state [40] and transitional [41] locomotion behaviors through complex terrain is substantially improved by leg touchdown detection.

Recently, conventional legged robot designers have embraced the virtue of sensor-minimal contact detection through proprioception — sensing embedded in the actuator itself — achieved through carefully transparent [42] or even direct [43] drive trains. Tendon-driven proprioception of contact in the quasi-static regime can be implemented by measuring tension [44]. However, dynamical operation requires rapid enough reaction that any delay in re-establishing cable tension after unloading through a contact event can be expected to interact with the time constants of the control loops being regulated. Our hopper applies a recently generalized notion of actuator "transparency" [45] to this unconventional drivetrain where the traditional notions of reflected inertia [42] do not seem directly applicable.

C. Contributions and Organization of the Paper

Our prior work [30] demonstrated that a REBO structure could be used to juggle (repeatedly loft and catch) a 1kg load. Here, we modify that design to achieve actual locomotion: translation of the mechanism's mass center through a two degree-of-freedom workspace. For purely vertical hopping, a conventional scaling analysis could anticipate some necessary redesign: lofting the tripled load ($\sim 3\,\mathrm{kg}$ incurred by the mass of the motors, the frame securing them to the leg and the boom) to $\sim 0.25\,\mathrm{bl}$ above stance height requires $\sim 88\,\mathrm{N}$ of peak compression force to load the spring with the necessary $\sim 1.25\,\mathrm{J}$ energy store, achievable by suitable regearing of the motors.[4] However, it was not clear whether the consequently diminished proprioceptive transparency [42], [45] would necessitate the introduction of toe contact sensors to ensure an adequate reaction time. More critically, prior kinematic analysis [30] showed that the range of motion and tracking error of the juggler's end effector was not adequate for the stepping control underlying fully planar locomotion via fore-aft hopping [8]. Together, these three design improvements — careful regearing; increase of workspace volume; and improved tracking control — yield the following new contributions:

- the design of a highly energetic, stable 2-DoF (planar) hopper with an origami leg capable of specific resistance [24], [25] as low as 1.6;
- experimental validation of the robot hopping with controllable height and forward speed over thousands of cycles; and
- the use of internal actuator (shaft encoder) signals to achieve purely proprioceptive contact detection in a tendon driven dynamically dexterous robot, showing potential to decrease system complexity.

Section II briefly reviews the origami leg design. Section III describes the mechanism and kinematic model of the hopping robot. Section IV presents the results of the robot performing vertical and fore-aft hopping. Section V describes our approach to proprioceptive contact sensing and Section VI concludes with a brief discussion of future research directions.

II. Origami Module Design

Reconfigurable Expanding Bistable Origami (REBO) pattern [2] is an origami tessellation conferring upon its folded form to store energy in both the folds and the faces. Its fold pattern is a function of geometric parameters a, b, stage height Δz and cone angle β, and is repeated in n_c columns and n_r rows[5], as shown in the left side of Fig. 1. We construct the origami bellow out of 8 mil thick Durilla synthetics paper with polyester finish (CTI Paper, USA) and glued into a closed cylinder with the 3M 467MP adhesive transfer tape. Our previous work [30] shows that these REBO bellows exhibit the compliance (force-extension) properties of a Hooke's law spring when compressed up to 2/3 of its travel. Data presented in [30] demonstrate that varying the cone angle β varies the REBO's stiffness, K_s, according to a roughly affine function $K_s(\mathrm{N\,m^{-1}}) = 16.1\beta(^\circ) - 43.7$. Furthermore, concentric arrangement of two REBOs as depicted in the right hand image of Fig. 1 achieves additive stiffness [30]. REBO mechanisms exhibit high resilience and tolerate repeated loading and unloading over thousands of cycles with little fatigue and no signs of physical damage, encouraging their use as a lightweight, ideal spring. The parameters for the double-layer REBO spring used in this research are given in Table I, where each REBO spring exhibits a stiffness of $K_s = 1035\,\mathrm{N\,m^{-1}}$. By arranging three of these double layer REBO springs in parallel, we get a compliant leg with stiffness of roughly $K_{es} = 3105\,\mathrm{N\,m^{-1}}$.

III. Hopper Robot Design

A. Robot Platform

The REBO Hopper robot shown in Fig. 2 uses the REBO bellows for energy storage and release during hopping. The design is a modification of the REBO Juggler in our previous work [30], where we turned the robot upside-down such that instead of pushing a ball into the air, the new robot pushes itself off the ground. The REBO Hopper comprises three major subsystems: (a) the compliant leg, (b) a toe sensor,

[4]The energy required for steady hopping at $5\,\mathrm{cm}$ for the $2.5\,\mathrm{kg}$ robot is $U = mgh = 1.25\,\mathrm{J}$, assuming that all energy is stored in the REBO spring with an effective stiffness of $K = 3105\,\mathrm{N\,m^{-1}}$, the spring is required to compress $\Delta x = \sqrt{2U/K} = 0.28\,\mathrm{m}$, meaning the force needed to hold the spring in storage position is $F = K\Delta x = 88\,\mathrm{N}$.

[5]The notation of the pattern has been changed from the previous work [30] to make the parameter more clear. The subscript (i or o) of the cone angle β, the length parameter a, b and h indicates the inner and the outer layer of the double-layered REBO structure. The number of the repeated column and row of the patterned is changed to n_c and n_r, respectively.

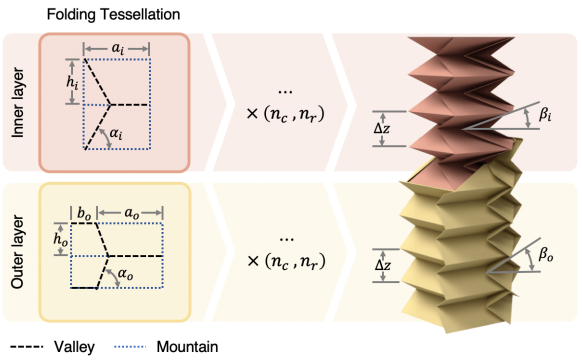

Fig. 1. Double-layered REBO mechanism. The left subplot shows the folding tessellation of the REBO structure, where it is repeated in n_c columns and n_r rows. The right subplot is the CAD rendering of the double-layered REBO, composed of two layers with different pattern parameters of the left subplot. The outer layer folded sheet is shown in yellow with a cutaway to better show the inner layer, shown in pink.

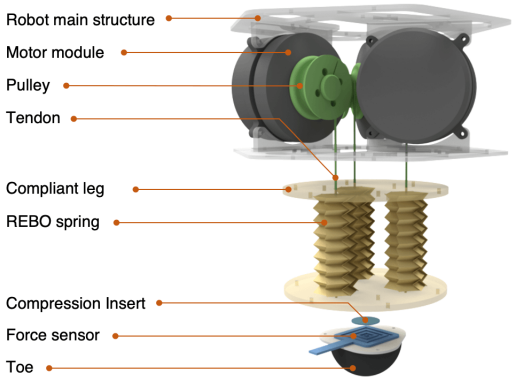

Fig. 2. CAD rendering of the REBO Hopper. The design is an inverted version of the REBO Juggler [30].

and (c) the mechatronic system with a microprocessor (Ghost Robotics MNS043 mainboard [46]) and a off-board 16V battery. The specifications of the robot are given in Table I.

Similarly to the previous design [30], each REBO linear actuator is made of a double-layered REBO spring with a tendon (Sufix 832 Advanced Superline Braid) laced through its structural through-holes, using the pulley mounted on a brushless DC electrical motor (Ghost Robotics MNSB01 Sub-Minitaur U8 Motor Module [46]) to control the compression of the REBO spring. With smaller pulley radius, the motor can provide greater force to compress the REBO spring; on the other hand, a larger pulley radius results in a faster response for pulling and releasing the spring. Here we design the radius of the pulley r_p to be 15 mm.

A compliant toe is mounted to the bottom of the spring and serves as the point of contact with the ground. The toe is a 3D printed hemisphere made of thermoplastic polyurethane (TPU) (TRONXY, part number Filament-TPU-TM) with a 10% infill. The result is a lightweight but highly damped toe. While the design of the toe is important, it is not the focus of this research, and we will show that even with this highly damped toe the REBO Hopper can still exhibit steady state hopping. A force sensor (Ohmite FSR01CE) is sandwiched

TABLE I
REBO HOPPER SPECIFICATIONS

Component	Properties
REBO spring (each)	
folding parameter	$\beta_o = 45°$, $a_o = 20\,\text{mm}$, $b_o = 5\,\text{mm}$, $\beta_i = 25°$, $a_i = 19\,\text{mm}$, $b_i = 0\,\text{mm}$, $\Delta z = 10\,\text{mm}$, $n_c = 6$, $n_r = 8$
rest length, l_0	77 mm
stiffness, K_s	$1035\,\text{N m}^{-1}$
mass, m_s	16 g
Compliant leg	
REBO circular pattern radius, d	35 mm
pulley radius, r_p	15 mm
leg stiffness, K_{es}	$3105\,\text{N m}^{-1}$
motor mass, toe mass (each)	350 g, 68 g
Robot	
height, width	230 mm, 210 mm
mass m_H, mass on the boom	2.53 kg, 3.2 kg

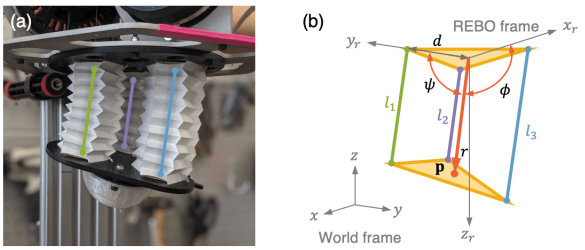

Fig. 3. (a) The compliant leg composed of REBO spring. (b) Kinematic model of the REBO Hopper's REBO linear actuator under compressive load, the model is an inverted version to the one for the REBO Juggler [30].

between the toe and a compression insert connected to the compliant body but we will show in Sec.V that the intrinsic transparency of the actuator itself [42], [45] is enough to achieve (at least purely vertical) hopping without recourse to this additional device.

B. Kinematic Model

The compliant leg (Fig. 3(a)) can be modeled as a three-link parallel manipulator, where two equilateral triangles form the base and the toe, respectively, and are connected at the corners by three tendons (Fig. 3(b)). The change of tendon length changes the position and orientation of the toe. Let the origin of the leg model be at the center of the top triangle, with $q_{la} = (l_1, l_2, l_3)$ being the state of the three parallel linear actuators. Then the state of the lower triangle can be described as $q_{lt} = (r, \psi, \phi) := f_2(q_{la})$[6] [30]:

$$
\begin{aligned}
r &= \tfrac{1}{3}(l_1 + l_2 + l_3) \\
\psi &= \cos^{-1}\left(\tfrac{1}{6d}(-2l_1 + l_2 + l_3)\right) \\
\phi &= \cos^{-1}\left(\tfrac{1}{2\sqrt{3}d}(-l_2 + l_3)\right).
\end{aligned}
$$

where r is the length of the vector $\mathbf{p}$ from the origin to the center of the lower triangle, ψ is the angle between $\mathbf{p}$ and the y_r axis, and ϕ the angle between $\mathbf{p}$ the x_r axis.

[6]The state of the lower triangle can be in comparison to the state of the top plate in our previous work, however, the symbol of the state had been changed from (r, θ, ϕ) to (r, ψ, ϕ)

TABLE II
SETPOINT CONTROL WITH PD CONTROLLER

Robot	measured (desired) compression in mm**				max error
Juggler [30]	9.5 (11),	12.5 (14),	15.2 (17),	17.2 (20)	14.0%
Hopper	14.0 (15),	18.7 (20),	23.4 (25),	28.2 (30)	6.6%

**The measurements are taken before performing hopping task as shown in previous work [30] Fig. 6(d) and this work's Fig 4(d). Four different desired setpoints are chosen and their corresponding measurements are recorded for the two different robots.

The experiments reported in this paper fix the REBO hopper on the one degree-of-freedom vertically sliding cart depicted in Fig. 4(a), and on the boom depicted in Fig. 5(a) admitting an additional (fore-aft) degree-of-freedom. For both behaviors, the pitch and roll orientations of the robot are fixed and the toe of the robot is set to move only in the $y_r z_r$-plane (i.e., $\phi = 0$). We define the state of the hopper as $q_h = (p_c, \theta) := f_h(q_{lt})$, where $p_c = l_0 - r$ is the compression of the REBO spring having a rest length of l_0, and $\theta = \pi/2 - \psi$ is the angle of $\mathbf{p}$ to the z_r axis on the sagittal $y_r z_r$ plane of the REBO frame in Fig. 3(b). For vertical hopping, we include the additional simplification that $\psi = 0$.

C. Control

The hopper is controlled by 3 DC motors with state defined as $q_m = (\theta_{m,1}, \theta_{m,2}, \theta_{m,3})$, and the mapping from the motor space to the REBO linear actuator, $q_{la} := f_1(q_m)$, is $l_i = l_0 + r_p \theta_{m,i}$, $i = 1, 2, 3$. The control command is generated by the desired state of the robot using inverse kinematics $q_m = f_1^{-1} \circ f_2^{-1} \circ f_h^{-1}(q_h)$. A PD feedback control loop is implemented on the motor for position control with encoder data. We have given the actuator some desired position command and measured the error. A comparison of position control error between the REBO Juggler [30] and REBO Hopper is shown in Table II. The maximum set point error in our previous work [30] is 14.0% due to the mechanical bias by the force created from the REBO spring. In this work, we have reduced the r_p to half the size to increase the force the motor can generate, thus reducing the maximum set point error to 6.6%. This set point error can be thought of as a result in offsetting the REBO rest length with the PD gains. The change in pulley size also provided us the capability to utilize more displacement with the spring, from only 22% of travel to 36%.

IV. DYNAMICAL HOPPING

A. Vertical Hopping

We tasked the REBO Hopper with 1 DOF open-loop vertical hopping to test its dynamic ability. The robot is mounted on a linear rail to constrain it to vertical motion. This is analogous to its capability to juggle a heavy shot ball, shown previously in our work with the REBO Juggler [30]. The three REBO springs of the hopper compress equally in order to store elastic energy based on the amount of compression. Effectively, this is similar to compression of a single spring with stiffness coefficient equal to sum of stiffness of all three springs. A slow motion video of 120 fps has been filmed for every trial and the trajectory of the hopper was measured using "Tracker" (https://physlets.org/tracker/).

The REBO Hopper is governed by the state machine depicted in Fig. 4(b), where the REBO actuator mode is controlled using toe force data as the guard condition, and the robot mode is the explicit hybrid dynamic behavior with the interaction of the environment. Initially, the REBO Hopper is held above ground and the tendon-pulley system coupled with the motor is used to compress the REBO spring to a length of p_{pc}, storing potential energy in the robot. When dropped, the toe sensor detects ground contact and shifts the control state machine to the stance mode where the REBO spring returns to its release mode, or the original zero-compression condition. Owing to the high stiffness of the structure, the decompression of the REBO springs is almost instantaneous when the tendon-pulley system is relaxed. This immediate thrust imparts the energy the hopper requires to lift off. Once the toe sensor detects lift-off from the ground, the control state-machine progresses the REBO actuator to the compress mode, bringing the robot to flight mode simultaneously. In this mode, the motors pre-compress the springs once more so that the robot is ready to hop at its next impact with the ground. Note that the flight/stance mode of the robot and the compress/release mode of the REBO actuator is equivalent in this state machine, since we assume the touchdown and liftoff event detected by the toe force sensor is the ground truth guard. An example of the mode switching using the torque sensor data is shown in Fig.4(c), where a trigger force value, τ_{tr}, was chosen for mode switching. The background colors of the plot also show current robot mode (yellow for stance, white for flight).

The relation between REBO spring compression length and apex height of steady state robot hopping was experimentally determined and shown in Fig. 4(d). We observe a monotonic increase in apex hopping height with increasing compression values as expected since we are increasing the robotic system's internal energy on contact as first proposed and empirically demonstrated in [8] and corroborated analytically in [47]. The motors used in the Hopper rotate at high speeds so that the compression and decompression actions occupy a very short time of flight or stance mode and do not interfere with its natural hopping frequency. The energetic properties of the REBO spring with respect to its work on the robot is as follows. The energy loaded into the REBO structure by the (brushless DC motor) motors' pre-compression work is $E = \frac{1}{2} K_{es} p_{pc}^2 = \frac{1}{2}(3105)*(0.0281)^2 \approx 1.23\,\mathrm{J}$ for the $2.5\,\mathrm{kg}$ hopper bouncing at a height of $56\,\mathrm{mm}$. Since the "release" mode has a typical duration of $60\,\mathrm{ms}$ the REBO delivers a mechanical power output of $20\,\mathrm{W}$. We will show in Sec. V that the robot can achieve a similar steady state hopping result with proprioceptive contact detection using only the shaft encoder of the driving motor.

We tested the ability of the REBO Hopper to enter an asymptotically stable hopping cycle by dropping it initially from different heights (the initial states) and observed that it did successfully transition to steady state hopping within 5

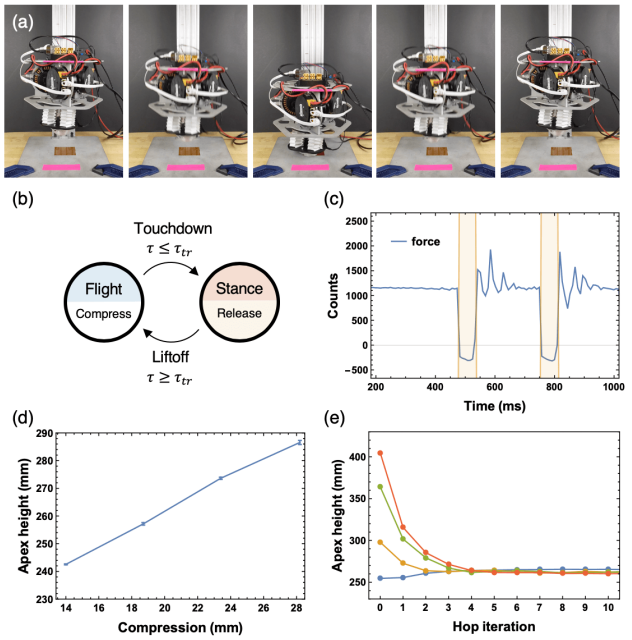

Fig. 4. Vertical hopping using toe force sensor (a) Snapshots of the experiment with an interval of 1/30 sec. (b) Hopping state machine, where the lower semi-circle of the node denotes the controllable REBO actuator mode, and the upper semi-circle the accompanying robot mode. (c) Toe sensor force data and REBO modes. The toe sensor force (ADC counts) was offset so that its touchdown events occur at the zero crossing, with the yellow shaded area representing stance mode (release mode of the REBO spring). (d) Steady-state hopping apex height using different REBO spring compression in compress mode. Measured using about 20 hops each. The largest STD, 0.7 mm, is very small compared to the overall apex height. (e) Transient responses (apex height w.r.t. hop iteration) from a variety of initial heights, exhibiting the asymptotically stable fixed point around 273.6 mm associated with the 23.4 mm compression in flight plotted in (d).

iterations, as shown in Fig. 4(e).

B. Fore-aft Hopping

Leveraging the vertical hopping controller and state machine and the leg's three DOF, the REBO Hopper was able to impart forward thrust using a SLIP-like behavior [48]. The REBO hopper was affixed to a boom with a locked pitch to simulate two DOF motion on the sagittal plane. The leg's kinematics were restricted in the controller to only allow angular (θ) and radial (r) motion, reducing the kinematic workspace of the hopper from the full three DOF (Fig. 3(b)) to the two DOF sagittal plane. Two different strategies were used to demonstrate the REBO hopper's capabilities: an open-loop set touchdown and a closed-loop Raibert-style fore-aft control [8]. Both strategies had two modes, flight and stance (as before), and both used the force sensor to detect touchdown and liftoff.

The open-loop control strategy is as follows: in flight, the hopper sets a fixed touchdown angle θ_{td} and compression magnitude $p_{c,td}$ and, in stance, the REBO leg is released producing radial and torsional forces propelling the leg forward. With this strategy, the robot can be commanded to travel in either direction and make qualitative adjustment to its velocity (faster, slower). In Fig. 5(b), the REBO Hopper was allowed to hop the entire circumference of the boom

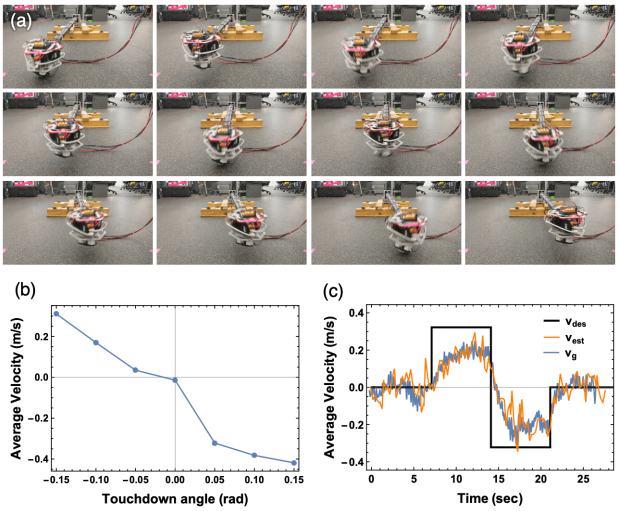

Fig. 5. Fore-aft Hopping (a) Snapshot of the experiment with an interval of 1/10 sec, left to right, top to bottom. (b) Average velocity over a lap around the boom containing 20 to 30 hopping cycles w.r.t. touchdown angle under open-loop control. (c) REBO hopper step response using Raibert-like feedback velocity control (Eq. 1). REBO tracks the desired velocity (v_{des}, black) with on-board touchdown velocity estimate (v_{est}, orange). Also shown is a (filtered) ground truth velocity measurement (v_g, blue).

and the steady state condition is shown. The relationship of angle and velocity is monotonic as expected. The mechanical power output of the REBO Hopper for the fore-aft motion is roughly the same as the vertical hopping with 20 W (with a pre-compression of 0.028 m), as shown in Sec. IV-A. Specific resistance can be calculate as $SR = P/(mgv) = 20\,\mathrm{W}/(3.2\,\mathrm{kg} * 9.8\,\mathrm{N\,m^{-1}} * 0.4\,\mathrm{m\,s^{-1}}) = 1.6$.

A Raibert-style [8] closed-loop control strategy was implemented for velocity regulation. In flight, the touchdown leg angle θ_{td} is set to an approximate neutral angle (a simplified proportional law feed forward term similar to the one used in [8], Eq. 2.4) with a P-loop controller around fore-aft velocity error (using an external encoder on the boom to estimate current velocity),

$$\theta_{td} = \frac{\dot{x}T_s}{2} + k_{\dot{x}}(\dot{x} - \dot{x}_{des}). \quad (1)$$

This strategy allowed the hopper to actively change velocity and resist significant (manual and step) perturbation. In Fig. 5(c), the hopper is given a set of velocity set-points as a step function. The hopper tracks to the set-points barring noisy velocity estimates, expected steady state offsets, and a small mechanical bias. In particular, the leg mechanism tendons were fastened in such a way that they could slip significantly affecting kinematic calculations and hindering the controllable fore-aft motion instead biasing the robot to one side.

This work does not focus on the fore-aft control, and as such an onboard velocity estimator was not built. Some velocity estimation should be possible without added sensors taking advantage of proprioception from the next section and the kinematics. This design exists as a proof of concept for the REBO actuation methods and future designs would focus on these lessons learned.

V. Proprioception with Tendon-Driven Actuator

In most tendon-driven systems actuated by a motor, disturbances can be measured at the end effector as long as the tendon remains in tension, as in the quasi-static regime [44]. However, when the tendon loses tension, the motor becomes decoupled from the end effector and loses information about the end effector's position, especially if the motor has low transparency as in a servo or highly geared motor and the system is operating in a dynamic regime. We propose a method of proprioception using the same actuator that drives the tendon to also detect contact. The REBO actuator can be considered as a physical spring in parallel with a virtual spring by virtue of the proportional control of the motor. As two springs load each other, the PD-controlled system will reach an equilibrium with the material spring, and the internal forces balance, resulting in a steady state motor position error as mentioned in Sec. III-C. In such a state, if a compressive disturbance (such as a touchdown impact) is introduced in the physical spring, the tendon will lose tension, allowing the virtual spring to return toward its desired position. By detecting this reaction from the proportional controller on the relatively small inertia of the motor and pulley, we can detect sudden contact. In this section we perform a collision test to determine the time delay between this proprioceptive contact detection and the toe force sensor and explain our findings using simple models. We show that this method of contact detection is sufficient for vertical hopping, despite the absence of a physical contact sensor.

A. Actuator Transparency and Contact Detection

We implement the proprioceptive contact detection as follows. Assign a desired pre-compression p_{pc} to the robot leg, after turning on the robot, read the encoder value and save this as the nominal pre-compression $\hat{p}_{pc}$ and set the trigger of contact detection to be $p_{tr} = \hat{p}_{pc} - \epsilon_{tr}$. Once the encoder value p_c is less than p_{tr}, we define the robot as having contacted the ground.

We perform a collision drop test similar to the one done in [45] to test out how different energy in this system affects the time delay of contact detection. The experiment uses the vertical hopping setup mentioned in Sec. IV-A. The robot is set to drop from different heights representing different collision energy input onto the floor while holding the REBO spring in different pre-compression p_{pc}. The toe sensor is used as the ground truth for detecting collision to the floor, and the time stamp is recorded as t_g. Once the robot detects contact using the proposed proprioceptive contact detection with $\epsilon_{tr} = 0.3\,\mathrm{mm}$, the time stamp is reported as t_p. Time delay is defined as $t_d = t_p - t_g$. A single trial is displayed in Fig. 6(a).

Fig. 6(b) shows the result of the drop collision test. Collision energy is defined as the potential energy from the drop height, $U_h = m_H g \Delta h$. Each data point in the figure is an average time delay of five collision drops. We can see that the result shares the similar trend as [45], where greater collision energy results in shorter time delay due to the extra energy available to allow the reflected inertia of

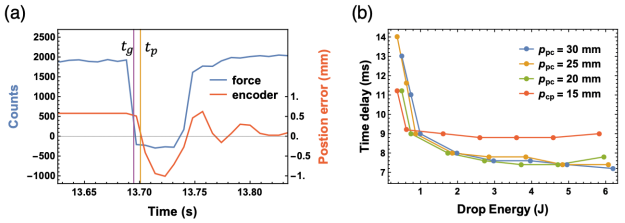

Fig. 6. Collision test for actuator transparency (a) Trajectory of toe force sensor (blue) and position error (red) both shifted so that the touchdown detection threshold is zero. Both touchdown events are highlighted: toe force touchdown detection t_g (purple) and proprioception touchdown detection t_p (yellow). (b) Detection time delay $t_d = t_p - t_g$ as a function of drop energy of the robot $U_h = m_H g \Delta h$.

the actuator to return to its original setpoint much faster. There is a cut off at the low energy where the robot will not detect contact at all since the position error is not enough to exceed the trigger value. The overall trend and value for different pre-compression to the REBO spring seems to be the same, except the lowest $p_{pc} = 15\,\mathrm{mm}$. We believe this is because the tension acting on the motor pulleys is lower in the case of 15 mm compression, where the steady state error is also lower, and in turn the motors return to desired angular position with a lower acceleration. As a result, at ground impact, the motors overshoot p_{tr} with a higher time delay. The stance mode of the robot is about $60\,\mathrm{ms}$, and there is enough time for the robot to detect contact using proprioception even with the lowest drop energy tested in this experiment.

Using a P-loop controller for proprioceptive measurements (as seen in Eq. 1 of [45]) and similarly written as

$$I\ddot{\theta} = k_p(\theta_{des} - \theta) \tag{2}$$

works well in both the drop test and the tendon losing tension. In Fig. 6(b) there is a similar trend to those seen in Fig. 2(a) from [45] and in fact, the time delay seems to improve for the tendon driven system. While the improvement is useful, it is not in the scope of this work to directly compare the magnitudes of energy and time between the two types systems.

B. Hopping with Proprioception

We conduct the vertical hopping test using the proprioceptive contact detection as the mode guard. The state machine is shown in Fig. 7(b), similar to Fig. 4(b). We have chosen $p_{tr} = 0.3\,\mathrm{mm}$ as our trigger for contact detection. When the hopper is in flight, the REBO actuator is in the compressed mode where the springs are set to a pre-compressed length p_{pc}. When the toe of the robot contacts the ground, i.e., the touchdown event, the robot enters stance mode. Once the proprioceptive contact detection gets triggered, the REBO actuator is set to be in release mode to relax to its rest length. Since contact detection using proprioception requires time to sense, the mode of the REBO actuator changes after the hopper is in stance mode. To make the state machine simple, the duration of the release mode of the REBO actuator is set to be $50\,\mathrm{ms}$, then the REBO actuator is switched to compressed mode. Since the REBO actuator is forced to

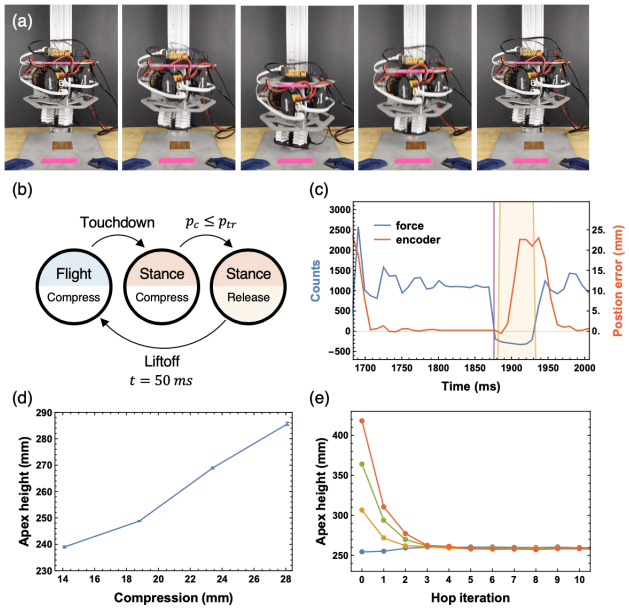

Fig. 7. Vertical hopping with proprioception (compare to toe sensor based hopping data, 4(b). (a) Snapshot of the experiment with an interval of 1/30 sec. (b) Hopping state machine, where the lower semi-circle of the node denotes the controllable REBO actuator mode, and the upper semi-circle denotes the resulting robot mode. (c) Toe sensor force data, the position error, and the REBO modes. The toe sensor force (ADC counts, blue) and the position error (mm, red) were both offset so that their respective touchdown events occur at the zero crossing. The purple vertical line represents the timestamp of ground truth contact from the force sensor. The stance mode (REBO release) starts when when the position error crosses zero shortly after true impact and is represented with the yellow shaded area. (d) Steady-state hopping apex height using different REBO spring compression length in compress mode and proprioceptive touchdown detection. (e) Transient responses (apex height w.r.t. iteration) of the hopper from a variety of initial heights, exhibiting the asymptotically stable fixed point around $268.9\,\mathrm{mm}$ associated with the $23.4\,\mathrm{mm}$ compression.

compress according to time duration, the spring may not have enough time to fully release. However, this Raibert's style hopping where the thrust injection is being implemented for a certain duration [8] has been proven to produce steady state hopping [47] and our experiment shows successful steady state hopping as well. The robot is forced to enter flight mode with the compress mode of the REBO actuator. Fig. 7(c) shows an example of mode selection using proprioception, where there is a gap between the ground truth and the estimated contact, as foreshadowed in the collision test. The time delay is small compared to the overall stance mode.

Fig. 7(d) shows the result of the hopping task with different pre-compression and their steady state apex hopping height. The result shows that the apex height is also monotonic in the compression length, as in the vertical hopping test with the toe sensor. The steady state apex height is slightly lower than the experiment using toe sensor. This is due to the fact that the energy injected to the system is for a fix duration and is sometime shorter than the stance duration of the hopping test with toe sensor. Take the hopping test using $p_{pc} = 25\,\mathrm{mm}$ compression for example, in Fig. 4(c), the stance mode is roughly $60\,\mathrm{ms}$, longer than the fixed duration shown in Fig. 7(c), suggesting that less energy is being injected into the hopper. Fig. 7(e) shows the wide basin of attraction of the hopping controller, where the robot dropped from different initial heights converges to the same apex height after around 5 iterations, showing the asymptotic stability of the hopping control with the proprioceptive feedback. Similarly, while the supplementary video submitted with this manuscript demonstrates robust hopping over both obstacle-cluttered and highly damped terrain, experimental data documenting these capabilities will be included in the final version of the paper.

VI. Discussion and Future Work

The stable steady vertical and fore-aft hopping of the REBO leg with reasonable energetic efficiency brings us closer to implementing the compliant origami structures in a functioning robot. Specifically, work in progress incorporates multiple REBO hoppers in the body of a quadruped robot, implementing compositional gaits [49] while maximizing the mechanical power output of the REBO devices. The successful implementation of proprioceptive contact detection reassures us that sensor-minimal approaches can be effective in such tendon-driven machines.[7]

We are also investigating alternative actuators — such as integration of new active materials into the base origami sheets — to greatly increase the power density by avoiding the framing cost of conventional electromagnetic motors, which could be a gateway to more energetic dynamical operation with heavy loads on a light energy storing structure.

Acknowledgment

This work is supported in part by the Army Research Office (ARO) under the SLICE Multidisciplinary University Research Initiatives (MURI) Program, award #W911NF1810327 and the National Science Foundation (NSF) grant #1845339. We thank Young-Joo Lee and Yuchong Gao for their insight in material properties, Jeremy Wang and Yifan Yuan for their help in fabrication, and Shane Rozen-Levy for his consulting on soft robotics literature. We also thank Diedra Krieger for her administrative support.

References

[1] B. Brown and G. Zeglin, "The bow leg hopping robot," in *Proceedings. 1998 IEEE International Conference on Robotics and Automation (Cat. No. 98CH36146)*, vol. 1. IEEE, 1998, pp. 781–786.

[2] H. Yuan, J. H. Pikul, and C. Sung, "Programmable 3-d surfaces using origami tessellations," in *7th International Meeting on Origami in Science, Mathematics, and Education*, 2018, pp. 893–906.

[3] D. M. Sussman, Y. Cho, T. Castle, X. Gong, E. Jung, S. Yang, and R. D. Kamien, "Algorithmic lattice kirigami: A route to pluripotent materials," *Proceedings of the National Academy of Sciences*, vol. 112, no. 24, p. 7449–7453, 2015.

[4] K. Lynch and M. Mason, "Dynamic underactuated nonprehensile manipulation," in *Proceedings of IEEE/RSJ International Conference on Intelligent Robots and Systems. IROS '96*, vol. 2, Nov 1996, p. 889–896 vol.2.

[7] At the time of writing, proprioceptive contact detection was working effectively for full planar (fore-aft hopping) locomotion. Space and time constraints have prevented us from presenting data beyond the purely vertical hopping discussed in Sec.V but work presently in progress will afford future opportunity for documenting the REBO's proprioceptive capabilities more completely.

[5] T. T. Topping, G. Kenneally, and D. E. Koditschek, "Quasi-static and dynamic mismatch for door opening and stair climbing with a legged robot," in *2017 IEEE International Conference on Robotics and Automation (ICRA)*. IEEE, 2017, pp. 1080–1087.

[6] D. E. Whitney, "Quasi-static assembly of compliantly supported rigid parts," *Journal of Dynamic Systems, Measurement, and Control*, vol. 104, no. 1, p. 65–77, Mar 1982.

[7] M. T. Mason, *Compliant motion*. MIT Press, 1982, p. 305–322.

[8] M. H. Raibert, *Legged robots that balance*. MIT press, 1986.

[9] R. Alexander, "Three uses for springs in legged locomotion," *International Journal of Robotics Research*, vol. 9, no. 2, p. 53–61, 1990.

[10] R. Altendorfer, N. Moore, H. Komsuoglu, M. Buehler, H. B. Brown, D. McMordie, U. Saranli, R. Full, and D. E. Koditschek, "Rhex: A biologically inspired hexapod runner," *Autonomous Robots*, vol. 11, no. 3, p. 207–213, 2001.

[11] D. M. Dudek and R. J. Full, "Passive mechanical properties of legs from running insects," *The Journal of experimental biology*, vol. 209, no. Pt 8, p. 1502–15, 2006.

[12] M. A. Daley, G. Felix, and A. A. Biewener, "Running stability is enhanced by a proximo-distal gradient in joint neuromechanical control," *J Exp Biol*, vol. 210, no. 3, p. 383–394, Feb 2007.

[13] J. W. Hurst and A. A. Rizzi, "Series compliance for an efficient running gait," *IEEE Robotics Automation Magazine*, vol. 15, no. 3, p. 42–51, 2008.

[14] Z. Shen and J. Seipel, "Animals prefer leg stiffness values that may reduce the energetic cost of locomotion," *Journal of theoretical biology*, vol. 364, p. 433–438, 2015.

[15] K. C. Galloway, J. E. Clark, and D. E. Koditschek, "Variable stiffness legs for robust, efficient, and stable dynamic running," *Journal of Mechanisms and Robotics*, vol. 5, no. 1, p. 011009–011009, Jan 2013.

[16] L. L. Howell, *Compliant mechanisms*. John Wiley & Sons, 2001.

[17] C. Laschi and M. Cianchetti, "Soft robotics: new perspectives for robot bodyware and control," *Frontiers in bioengineering and biotechnology*, vol. 2, p. 3, 2014.

[18] K. C. Galloway, J. E. Clark, and D. E. Koditschek, "Design of a multi-directional variable stiffness leg for dynamic running," in *ASME 2007 International Mechanical Engineering Congress and Exposition*. American Society of Mechanical Engineers, 2007, pp. 73–80.

[19] R. F. Shepherd, F. Ilievski, W. Choi, S. A. Morin, A. A. Stokes, A. D. Mazzeo, X. Chen, M. Wang, and G. M. Whitesides, "Multigait soft robot," *Proceedings of the national academy of sciences*, vol. 108, no. 51, pp. 20 400–20 403, 2011.

[20] S. Seok, C. D. Onal, K.-J. Cho, R. J. Wood, D. Rus, and S. Kim, "Meshworm: a peristaltic soft robot with antagonistic nickel titanium coil actuators," *IEEE/ASME Transactions on mechatronics*, vol. 18, no. 5, pp. 1485–1497, 2012.

[21] N. W. Bartlett, M. T. Tolley, J. T. Overvelde, J. C. Weaver, B. Mosadegh, K. Bertoldi, G. M. Whitesides, and R. J. Wood, "A 3d-printed, functionally graded soft robot powered by combustion," *Science*, vol. 349, no. 6244, pp. 161–165, 2015.

[22] M. T. Tolley, R. F. Shepherd, M. Karpelson, N. W. Bartlett, K. C. Galloway, M. Wehner, R. Nunes, G. M. Whitesides, and R. J. Wood, "An untethered jumping soft robot," in *2014 IEEE/RSJ International Conference on Intelligent Robots and Systems*. IEEE, 2014, pp. 561–566.

[23] T. Umedachi, V. Vikas, and B. Trimmer, "Softworms: the design and control of non-pneumatic, 3d-printed, deformable robots," *Bioinspiration & biomimetics*, vol. 11, no. 2, p. 025001, 2016.

[24] T. Von Karman and G. Gabrielli, "What price speed? specific power required for propulsion of vehicles," *Mechanical Engineering*, vol. 72, p. 775–781, 1950.

[25] P. Gregorio, M. Ahmadi, and M. Buehler, "Design, control, and energetics of an electrically actuated legged robot," *IEEE Transactions on Systems, Man, and Cybernetics, Part B (Cybernetics)*, vol. 27, no. 4, pp. 626–634, 1997.

[26] J. D. Weingarten, G. A. D. Lopes, M. Buehler, R. E. Groff, and D. E. Koditschek, "Automated gait adaptation for legged robots," in *2004 IEEE International Conference on Roboticsand Automation (ICRA)*, vol. 3. IEEE, 2004, p. 2153–2158.

[27] S. Seok, A. Wang, M. Y. M. Chuah, D. J. Hyun, J. Lee, D. M. Otten, J. H. Lang, and S. Kim, "Design principles for energy-efficient legged locomotion and implementation on the mit cheetah robot," *IEEE/ASME Transactions on Mechatronics*, vol. 20, no. 3, p. 1117–1129, 2015.

[28] J. L. Silverberg, A. A. Evans, L. McLeod, R. C. Hayward, T. Hull, C. D. Santangelo, and I. Cohen, "Using origami design principles to fold reprogrammable mechanical metamaterials," *science*, vol. 345, no. 6197, pp. 647–650, 2014.

[29] E. T. Filipov, T. Tachi, and G. H. Paulino, "Origami tubes assembled into stiff, yet reconfigurable structures and metamaterials," *Proceedings of the National Academy of Sciences*, vol. 112, no. 40, pp. 12 321–12 326, 2015.

[30] W.-H. Chen, S. Misra, Y. Gao, Y.-J. Lee, D. E. Koditschek, S. Yang, and C. Sung, "A programmably compliant origami mechanism for dynamically dexterous robots," *IEEE Robotics and Automation Letters*, vol. 5, no. 2, p. 2131–2137, Apr 2020.

[31] J. Santoso, E. H. Skorina, M. Luo, R. Yan, and C. D. Onal, "Design and analysis of an origami continuum manipulation module with torsional strength," in *2017 IEEE/RSJ International Conference on Intelligent Robots and Systems (IROS)*, Sep. 2017, pp. 2098–2104.

[32] E. Vander Hoff, D. Jeong, and K. Lee, "Origamibot-i: A thread-actuated origami robot for manipulation and locomotion," in *2014 IEEE/RSJ International Conference on Intelligent Robots and Systems*. IEEE, 2014, pp. 1421–1426.

[33] K. Zhang, C. Qiu, and J. S. Dai, "An extensible continuum robot with integrated origami parallel modules," *Journal of Mechanisms and Robotics*, vol. 8, no. 3, p. 031010, 2016.

[34] J. Carlson, J. Friedman, C. Kim, and C. Sung, "REBOund: Untethered origami jumping robot with controllable jump height," in *IEEE International Conference on Robotics and Automation*, 2020, (submitted).

[35] M. A. Erdmann and M. T. Mason, "An exploration of sensorless manipulation," *IEEE Journal on Robotics and Automation*, vol. 4, no. 4, p. 369–379, 1988.

[36] M. T. Mason, "Kicking the sensing habit," *AI Magazine*, vol. 14, no. 1, p. 58–59, 1993.

[37] R. M. Ghigliazza, R. Altendorfer, P. Holmes, and D. Koditschek, "A simply stabilized running model," *SIAM REVIEW*, vol. 47, no. 3, p. 519–549, 2005.

[38] J. C. Spagna, D. I. Goldman, P. C. Lin, D. E. Koditschek, and R. J. Full, "Distributed mechanical feedback in arthropods and robots simplifies control of rapid running on challenging terrain," *Bioinspiration and Biomimetics*, vol. 2, no. 1, p. 9–18, 2007.

[39] M. J. Spenko, J. A. Saunders, G. C. Haynes, M. R. Cutkosky, A. A. Rizzi, R. J. Full, and D. E. Koditschek, "Biologically inspired climbing with a hexapedal robot," *Journal of Field Robotics*, vol. 25, no. 4–5, p. 223–242, 2008.

[40] J. D. Weingarten, R. E. Groff, and D. E. Koditschek, "A framework for the coordination of legged robot gaits," in *2004 IEEE Conference on Robotics, Automation and Mechatronics*, vol. 2. IEEE, 2004, p. 679–686. [Online]. Available: http://ieeexplore.ieee.org/xpls/abs_all.jsp?arnumber=1438000

[41] T. T. Topping, V. Vasilopoulos, A. De, and D. E. Koditschek, "Composition of Templates for Transitional Pedipulation Behaviors," in *International Symposium on Robotics Research (ISRR)*, 2019.

[42] P. M. Wensing, A. Wang, S. Seok, D. Otten, J. Lang, and S. Kim, "Proprioceptive actuator design in the mit cheetah: Impact mitigation and high-bandwidth physical interaction for dynamic legged robots," *IEEE Transactions on Robotics*, vol. 33, no. 3, pp. 509–522, 2017.

[43] G. Kenneally, A. De, and D. E. Koditschek, "Design principles for a family of direct-drive legged robots," *IEEE Robotics and Automation Letters*, vol. 1, no. 2, pp. 900–907, 2016.

[44] B. Belzile and L. Birglen, "A compliant self-adaptive gripper with proprioceptive haptic feedback," *Autonomous Robots*, vol. 36, no. 1-2, pp. 79–91, 2014.

[45] G. Kenneally, W.-H. Chen, and D. Koditschek, "Actuator transparency and the energetic cost of proprioception," in *ISER*, 2018. [Online]. Available: https://repository.upenn.edu/ese_papers/862/

[46] "Ghost Robotics," https://www.ghostrobotics.io.

[47] M. Buehler and D. Koditschek, "Analysis of a simplified hopping robot," in *, 1988 IEEE International Conference on Robotics and Automation, 1988. Proceedings*, Apr 1988, p. 817–819 vol.2.

[48] R. Blickhan and R. J. Full, "Similarity in multilegged locomotion: Bouncing like a monopode," *Journal of Comparative Physiology A: Sensory, Neural, and Behavioral Physiology*, vol. 173, no. 5, p. 509–517, 1993.

[49] A. De and D. E. Koditschek, "Vertical hopper compositions for preflexive and feedback-stabilized quadrupedal bounding, pacing, pronking, and trotting," *The International Journal of Robotics Research*, vol. 37, no. 7, p. 743–778, Jun 2018.